Photoelectrochemistry of Composite Semiconductor Thin Films. Photosensitization of SnO_2/CdS Coupled Nanocrystallites with a Ruthenium Polypyridyl Complex

Chouhaid Nasr and Surat Hotchandani

Groupe de Recherche en Énergie et Information Biomoléculaires, Université du Québec à Trois Rivières, Trois Rivières, Québec, Canada G9A 5H7

Won Y. Kim and Russell H. Schmehl

Department of Chemistry, Tulane University, New Orleans, Louisiana 70118

Prashant V. Kamat*

Radiation Laboratory, University of Notre Dame, Notre Dame, Indiana 46556

Received: March 5, 1997; In Final Form: June 26, 1997[⊗]

The charge injection from an excited Ru(II) complex (viz., $(Ru(bpy)_2(L))^{2+}$, where L = 4-(2,2′-bipyrid-4-yl)phenyl diphosphonate) into SnO_2 and SnO_2/CdS films is investigated to elucidate the beneficial effect of composite semiconductor systems. The electrons injected from excited Ru(II) into CdS are transferred quickly into SnO_2 nanoclusters, thus promoting the charge separation. Photoelectrochemical measurements suggest improved photon to photocurrent charge carrier generation efficiency in the SnO_2/CdS composite system. The formation of the oxidation product, Ru(III), and the recovery of the sensitizer are investigated using transient absorption spectroscopy. The rate constant for the back electron transfer in the SnO_2/CdS/Ru(II) composite system is slower by a factor of 2−3 than the one observed in the SnO_2/Ru(II) system. The beneficial aspects of composite semiconductor systems in photochemical solar cells are presented.

Introduction

Photosensitization of semiconductor nanocrystallites with inorganic[1−4] and organic[5−9] dyes has created new enthusiasm in utilizing dye-modified semiconductor thin films for developing highly efficient photoelectrochemical cells.[10,11] Although ruthenium(II) polypyridyl complexes have been employed as efficient photosensitizers for the past two decades,[1−4,12−22] it has only been possible recently to achieve practically viable efficiencies in the range of 10%. Photochemical solar cells with net power conversion efficiencies up to 10% have been reported using a nanocrystalline TiO_2−Ru polypyridyl complex system.[2]

The energy difference between the conduction band of the semiconductor and oxidation potential of the excited sensitizer is the major driving force for the excited state charge transfer.[23,24] Different approaches have been considered to study the energy gap dependence of the photosensitization efficiency.[25−30] It is known that the photosensitization efficiency of a dye-modified semiconductor electrode is strongly dependent on the applied bias.[24] It significantly decreases when the applied potential is more negative to the flat-band potential of the semiconductor. In a recent study it was shown that the rate constant of charge injection became slower at potentials more negative than the flat-band potential of the semiconductor.

Similarly, the back-electron-transfer rate between the injected electron and oxidized sensitizer has been reported to be dependent on the applied bias[31,32] and excitation intensity.[33,34] An increase in the back-electron-transfer rate constant is directly reflected in a decrease in the photoconversion efficiency. This problem is especially serious in nanocrystalline semiconductor-based photoelectrochemical systems. The lack of potential gradient to drive away the injected charge toward the collecting surface becomes a major limiting factor in unbiased cells. This charge transport limitation within nanocrystalline semiconductor films can be overcome by applying an electrochemical bias.

SCHEME 1: Charge Injection from Excited Sensitizer (S*) into SnO_2/CdS Composite Semiconductor Nanoclusters

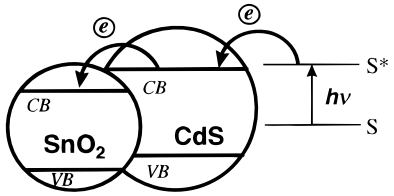

An alternate approach for improving charge separation is to employ composite semiconductor films consisting of two or more semiconductors with favorable energetics.[6,35] Up to 10 times enhancement in the photocatalytic degradation rates using SnO_2/TiO_2 composite films has been demonstrated in a recent study.[36,37] Coupling a large bandgap semiconductor with a smaller bandgap semiconductor not only extends the photoresponse into the visible but also facilitates charge separation by accumulating electrons and holes in separate particles. Improved charge separation in TiO_2/CdS,[38,39] SnO_2/CdS,[40] ZnO/ZnS,[41,42] and ZnO/CdS[35] has been demonstrated with transient absorption measurements. Similarly, a charge rectification effect has been demonstrated using TiO_2/CdSe and SnO_2/CdSe thin films.[43−47] Yet no major effort has been made to employ composite semiconductor systems in dye-sensitization systems.[6]

An example of dye sensitization of SnO_2/CdS composite system is shown in Scheme 1. CdS is a short bandgap semiconductor (E_g = 2.5 eV) with its conduction band (−0.8 V vs NHE) more negative than that of SnO_2 (0.0 V vs NHE). Upon excitation of the sensitizing dye, the electron is first injected into the CdS layer. The photoinjected electrons are

* Address correspondence to this author. e-mail: Kamat@marconi.rad.nd.edu or http://www.nd.edu/~pkamat.

[⊗] Abstract published in *Advance ACS Abstracts,* August 15, 1997.

S1089-5647(97)00833-X CCC: $14.00

then quickly transferred from CdS to SnO_2 nanocrystallites, thus decreasing the probability of back-electron-transfer process. To the best of our knowledge, this is first detailed study to highlight the usefulness of composite semiconductor system in Ru(II) polypyridyl complex based photochemical solar cells. In this paper, a series of photoelectrochemical and time-resolved transient absorption experiments are presented which serve to demonstrate the beneficial role of composite semiconductors for improving the performance of nanocrystalline semiconductor-based photochemical solar cells.

Experimental Section

Materials. Optically transparent electrodes (OTE) were cut from an indium tin oxide-coated glass plate (1.3 mm thick, 20 ohms/square) obtained from Donnelly Corp., Holland, MI. SnO_2 colloidal suspension (18%) was obtained from Alfa Chemicals and used without further purification.[48] The synthesis of Ru-(2,2′-bipyridine)$_2$(2,2′-bipyridine-5-phenyl diphosphonate)$^{2+}$, ((Ru(bpy)^{2}L)PF_6^-, is described elsewhere.[49] Absorption spectra were recorded with a Perkin-Elmer 3840 diode array spectrophotometer. Emission spectra were recorded with SLM S-8000C spectrofluorimeter.

Preparation of SnO_2 Particulate Films. The synthetic procedure for casting transparent a thin film of SnO_2 on an optically transparent electrode has been reported earlier.[4] A small aliquot (usually 0.5 mL) of the diluted SnO_2 colloidal suspension (0.18%) was applied to a conducting surface of 0.8 $\times$ 3 cm^2 of OTE and was dried in air on a warm plate. The SnO_2 colloid-coated glass plates were then annealed at 673 $\pm$ 25 K for 1 h. The thin film semiconductor electrode is referred to as OTE/SnO_2. The thickness of the film was ≤ 1 μm.

Modification with CdS. The procedure was similar to the one described in our earlier studies.[35] The nanostructured SnO_2 films cast on conducting glass plate (OTE/SnO_2 electrode) were surface modified with CdS by dipping them successively in $Cd(ClO_4)_2$ and Na_2S solutions. The electrodes were washed with deionized water between each dipping so that only adsorbed Cd^{2+} precipitated as CdS on the SnO_2 surface. The yellow coloration of the film confirmed the deposition of CdS nanocrystallites over SnO_2 particles. This chemical deposition method provides a convenient way to modify SnO_2 particles with a small bandgap semiconductor such as CdS. The SnO_2/CdS composite film thus consists of sequential layers of SnO_2 and CdS semiconductor nanocrystallites. The charges injected from excited CdS into the SnO_2 particles are efficiently transported to the collecting surface of OTE since SnO_2 layer is essentially an interconnected chain of nanocrystallites.

A Hitachi S-4500 scanning electron microscope (SEM) was employed to record the images of the nanostructured semiconductor films with 300 K magnification. The films were cast on conducting glass substrates (1 cm^2) using the procedure described above.

Modification with Ru(bpy)$_2$(L)$^{2+}$. We modified the OTE/SnO_2 and OTE/SnO_2/CdS electrodes with Ru^{II}(2,2′-bipyridine)$_2$-(4-(2,2′-bipyrid-4-yl)phenyl diphosphonate)) ((Ru(bpy)$_2$L)$(PF_6)_2$, referred in the text as Ru(II)) by dipping them directly in an acetonitrile solution containing Ru(II) complex for a period of 8−10 h. The electrode was then thoroughly washed with acetonitrile and stored in the dark. The deepening of the orange coloration of the nanoporous semiconductor film ($A_{470\ nm} \sim 0.3$) further confirmed adsorption of Ru(II) in large amounts. The methodology adopted for the electrode preparation is summarized in Scheme 2 (These electrodes will be referred to as OTE/SnO_2/Ru(II) and OTE/SnO_2/CdS/Ru(II) in the following discussion.)

SCHEME 2: Preparation of Ru(II)-Modified SnO_2/CdS Composite Semiconductor Films on a Conducting Glass Electrode (OTE)

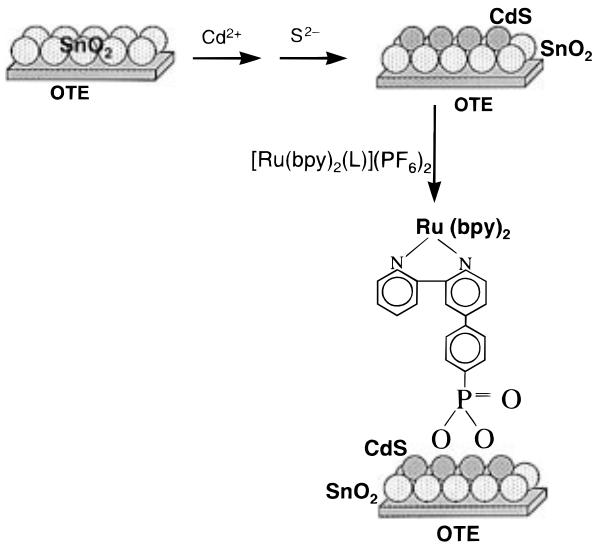

Photoelectrochemical Measurements. The measurements were carried out in a thin-layer cell consisting of a 2 or 5 mm path length quartz cuvette with two side arms attached for inserting reference and counter (Pt gauze) electrodes. We used 0.04 M I_2 and 0.5 M LiI in acetonitrile as electrolyte. The spectroelectrochemical cell employed in the present set of experiments is described earlier.[50] Photocurrent measurements were carried out with a Keithley Model 617 programmable electrometer. A collimated light beam from a 250 W xenon lamp was used as the light source. A Bausch and Lomb high-intensity grating monochromator was introduced into the path of the excitation beam for selecting the excitation wavelength.

Lifetime Measurements. Emission lifetime measurements were performed by time-correlated single-photon counting using an apparatus that has been described elsewhere.[51] The excitation source was a mode-locked, Q-switched Quantronix 416 Nd:YAG laser which provided 80 ps pulses of 355 nm light with a frequency of 5 kHz and an integrated power of 10 mW.

Laser Flash Photolysis Experiments. The spectroelectrochemical cell containing the Ru(II)-modified electrode was placed in the sample compartment of the nanosecond laser flash photolysis setup. The excitation was carried out in a front face geometry with 532 nm laser pulses from a Quanta-Ray CDR-1 Nd:YAG laser system (~6 ns pulse width, 5 mJ). The photomultiplier output was digitized with a Tektronix 7912 AD programmable digitizer. A typical experiment consisted of a series of 3−6 replicate shots per single measurement. The average signal was processed with an LSI-11 microprocessor interfaced with a VAX computer.[52]

Results and Discussion

Absorption Characteristics of Dye-Modified Nanocrystalline Semiconductor Electrodes. The chemical precipitation of CdS nanocrystallites on the nanostructured SnO_2 films was carried out using a procedure employed earlier for preparing TiO_2/CdS[53] and ZnO/CdS[35] composite films. The absorption spectra recorded during various stages of surface modification with CdS complex are shown in Figure 1A. The OTE/SnO_2 electrode absorbs only in the UV whereas CdS-modified SnO_2 films exhibit absorbance at wavelengths greater than 400 nm. With successive exposure of the OTE/SnO_2 electrodes to Cd^{2+} and S^{2-} ions a layer of CdS nanocrystallites is formed on the

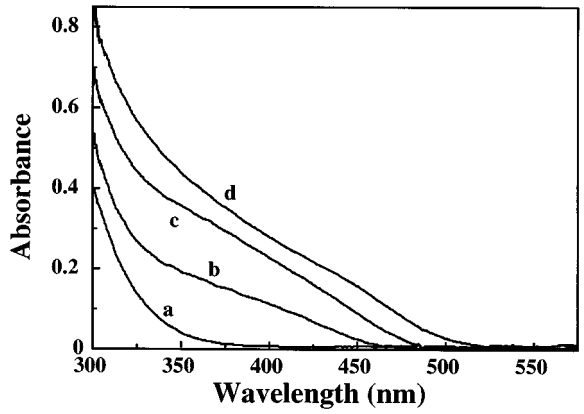

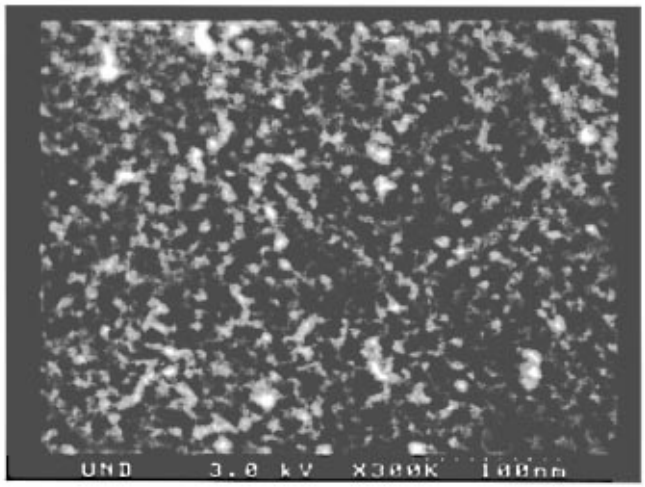

Figure 1. (A, top) Absorption spectra of OTE/SnO_2 electrodes at different stages of CdS capping. Spectra a−d were recorded following each cycle of successive dipping of OTE/SnO_2 in solutions $Cd(ClO_4)_2$ and Na_2S. (B, bottom) Scanning electron micrograph of SnO_2/CdS composite semiconductor film cast on a conducting glass substrate. The picture was recorded with a magnification of 300 000.

SnO_2 surface. The increase in the absorbance seen with such successive treatments confirms the growth of CdS on SnO_2 particles. No significant increase in the absorbance is seen after about five such treatments.

The scanning electron micrograph of chemically deposited CdS on SnO_2 film is shown in Figure 1B. As reported in our previous study, SnO_2 thin films consist of 5 nm diameter nanocrystallites.[4] The *grape bunch*-type clusters create nanostructured pores of various dimensions within the film. The CdS layer deposited on the SnO_2 film consists of 10 nm diameter spherical clusters. This CdS layer is relatively thin and consists of a layer of ~10 nm diameter particles closely interacting with the SnO_2 surface. The overall thickness of the sequential layers of SnO_2 and CdS is still around 1 μm. The surface modification of SnO_2 and SnO_2/CdS films with Ru(II) complex was achieved by dipping the respective electrodes in an acetonitrile solution containing the sensitizer overnight. The phosphonate group of the sensitizer facilitated strong binding of this complex to the semiconductor surface.

The Ru(II) complex absorbs strongly in the visible (ϵ_{460} = 15 500 M^{-1} cm^{-1}) and is able to sensitize large bandgap semiconductors such as SnO_2.[4] The absorption spectra recorded before and after the surface modification of OTE/SnO_2 and OTE/SnO_2/CdS electrodes are shown in Figure 2. The appearance of a strong absorption band at 470 nm confirms the binding of the sensitizer to the semiconductor surface. Such a surface modification also facilitates extension of the photoresponse of these Ru(II)-modified films beyond 550 nm.

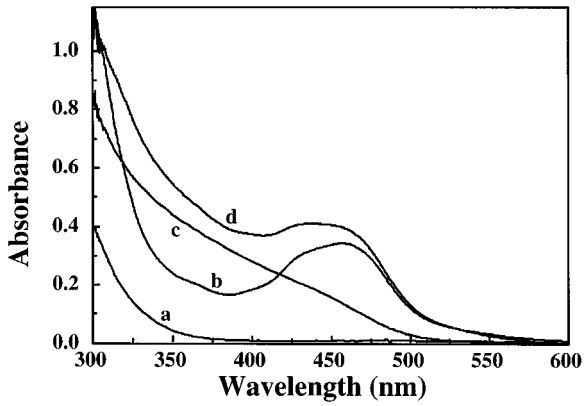

Figure 2. Absorption spectra of SnO_2 and SnO_2/CdS thin films before and after modification with Ru(II) complex: (a) OTE/SnO_2, (b) OTE/SnO_2/Ru(II), (c) OTE/SnO_2/CdS, and (d)OTE/SnO_2/CdS/Ru(II).

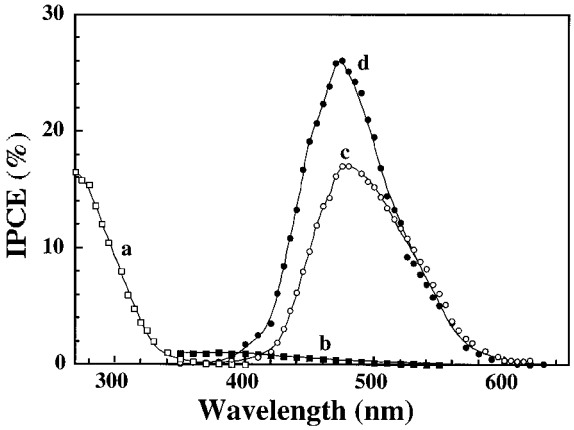

Figure 3. Photocurrent action spectrum of OTE/SnO_2 and OTE/SnO_2/CdS electrodes before and after modification with Ru(II) complex: (a) OTE/SnO_2 (electrolyte: 0.02 M, NaOH), (b) OTE/SnO_2/CdS (electrolyte: 0.04 M I_2 and 0.5 M LiI in acetonitrile) (c) OTE/SnO_2/Ru(II), and (d)OTE/SnO_2/CdS/Ru(II) (electrolyte: 0.04 M I_2 and 0.5 M LiI in acetonitrile.) IPCE (%) was determined from the expression {100(1240 i_{sc})/(λ I_{inc})}, where i_{sc} is the short-circuit current photocurrent (A/cm^2), I_{inc} is the incident light intensity (W/cm^2), and λ is the excitation wavelength (nm).

Photoelectrochemical Behavior of Ru(II)-Modified Electrodes. The photoelectrochemical properties of SnO_2 films prepared from colloidal suspensions is described in our earlier study. The high porosity of this film facilitates adsorption of Ru(II) in very high concentrations. The dye-modified semiconductor thin films exhibit excellent electrochemical and photoelectrochemical activity.[8,54] The SnO_2 films modified with Ru(II) exhibit incident photon-to-photocurrent efficiency (IPCE) in the range 20−25% and a light-harvesting efficiency as high as 50%.

Figure 3 shows the photocurrent response of OTE/SnO_2 and OTE/SnO_2/CdS electrodes before and after modification of Ru(II) complex. The OTE/SnO_2 electrode which is photoactive only in the UV region responds to the visible region (λ < 500 nm) upon modification with CdS. Both OTE/SnO_2 and OTE/SnO_2/CdS electrodes upon modification with Ru(II) complex exhibit a prominent peak around 470 nm. Please note that we deliberately introduced a 400 nm cutoff filter to block the near-UV excitation in order to avoid direct bandgap excitation of SnO_2 and CdS semiconductor nanocrystallites. The absorbance of Ru(II) at 470 nm (~0.3) is sufficiently higher than that of CdS layer (~0.1) so that the incident light at this wavelength is absorbed mainly by the sensitizer.

The action spectra of the Ru(II)-modified electrodes closely match the spectral features of respective electrodes presented

SCHEME 3: Mechanism of Dye Sensitized Photocurrent Generation in a Composite Semiconductor Film

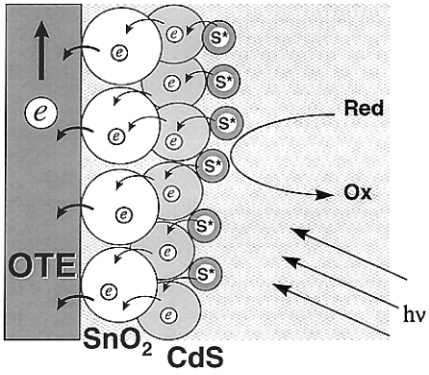

in Figure 2 and thus confirm that the photosensitization mechanism is operative in extending the photocurrent response of semiconductor thin film electrodes. The presence of redox couple such as I_3^-/I^- in the electrolyte facilitates quick regeneration of the sensitizer.

The mechanism of photosensitized current generation at a Ru(II)-modified composite film is illustrated in Scheme 3. The maximum IPCE of 28% at 480 nm obtained for OTE/SnO_2/CdS/Ru(II) is nearly 50% higher than that of OTE/SnO_2/Ru(II). This enhancement in IPCE cannot be a mere additive effect of contributions from CdS and Ru(II). Although CdS absorbs in the region where Ru(II) absorption dominates, we consider its contribution to be small. This is mainly because CdS film in contact with I_3^-/I^- couple shows very poor photocurrent generation. Therefore, we attribute the observed photocurrent generation to arise mainly from the absorption of the light by the sensitizer.

The enhancement in the photocurrent generation in the composite system and the ability to generate anodic photocurrent in a composite semiconductor film demonstrate the cascading flow of electrons from the excited sensitizer to CdS to SnO_2 and then to the collecting surface of OTE. A proper choice of composite semiconductor systems (e.g., SnO_2/TiO_2) is crucial for observing an enhanced efficiency. In fact, in one of our early studies we were able to achieve an order of magnitude enhancement in the IPCE of chlorophyll *a*-sensitized ZnO nanocrystalline film by coupling it with CdS.[6] In order to further explore the kinetic and mechanistic details of the sensitization of SnO_2/CdS semiconductor composites, we carried out time-resolved transient absorption and emission measurements.

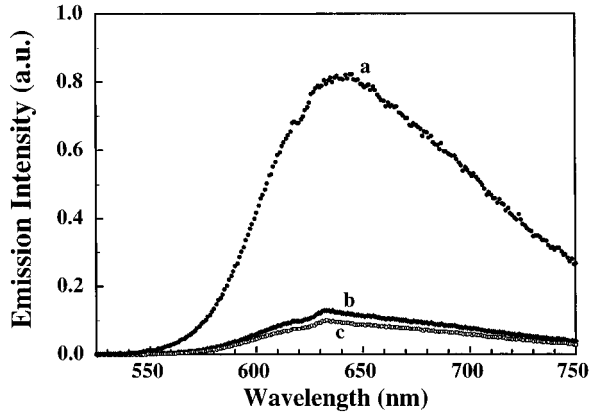

Figure 4. Emission spectra of (a) OTE/SiO_2/Ru(II), (b) OTE/SnO_2/Ru(II), and (c) OTE/SnO_2/CdS/Ru(II). Excitation was at 460 nm. The spectra were recorded in a front face configuration and are corrected for instrument response.

Quenching of Emission on Semiconductor Surfaces. The Ru(II) complex has a strong emission in the red region with a maximum around 640 nm. In Figure 4 the emission spectra of Ru(II)* on SnO_2 and CdS-modified SnO_2 films are compared with that on SiO_2 film. The absorbance at the excitation wavelengths was similar (0.10 ± 0.01) for all these samples. A nonreactive surface such as SiO_2 does not influence the deactivation of the excited state, and hence we observe its emission behavior to be similar to that in neat solvents. On the other hand, SnO_2 and SnO_2/CdS nanoclusters directly interact with the Ru(II) complex and quench the excited state. More than 80% decrease in emission yield is seen in these two cases. As shown earlier, such a decrease in emission yield represents the fraction of the excited state sensitizer participating in the charge injection process.[55−57] The excited state processes of Ru(II) are summarized in reactions 1−3.

$$\text{Ru(II)} + h\nu \rightarrow \text{Ru(II)}^* \xrightarrow{k_r} \text{Ru(II)} + h\nu' \quad (1)$$

$$\text{Ru(II)}^* \xrightarrow{k_{nr}} \text{Ru(II)} \quad (2)$$

$$\text{Ru(II)}^* + \text{SnO}_2 \xrightarrow{k_{et}} \text{SnO}_2(\text{e}) + \text{Ru(III)} \quad (3)$$

Since Ru(II)* deactivates via radiative (k_r), nonradiative (k_{nr}), and electron transfer (k_{et}) processes, one can express the quantum yields for emission and net electron transfer processes by expression 4.

$$\Phi_r = k_r/(k_r + k_{nr} + k_{et}) \quad \text{and} \quad \Phi_{et} = k_{et}/(k_r + k_{nr} + k_{et}) \quad (4)$$

For Ru(II)* adsorbed on SnO_2 nanocrystallites one can correlate the two quantum yields with expression 5.

$$\Phi_r + \Phi_{et} = \text{constant} \quad (5)$$

If nonradiative decay remains unaffected on different semiconductor surfaces, one can expect a decrease in Φ_r to reflect an increase in Φ_{et}. From the observed decrease in emission quantum yield, one can obtain the maximum limit for the electron injection efficiency of a given semiconductor/dye system. In the present experiments the net electron injection efficiency was greater than 80% for both Ru(II) adsorbed on SnO_2 and SnO_2/CdS composite films.

The emission lifetimes are useful for obtaining the kinetic details of heterogeneous electron transfer between the semiconductor and sensitizer (reaction 3). Figure 5 shows the emission decay of Ru(II)* adsorbed on SiO_2, SnO_2, and SnO_2/CdS surfaces. Since CdS also absorbs 355 nm laser pulse, we checked the emission arising from its direct excitation. Blank experiments carried out with SnO_2 or SnO_2/CdS films did not produce any detectable signal in the time scale of our measurements. (Although CdS clusters emit weakly in the red, CdS-capped SnO_2 colloids do not. The interaction between the two semiconductor systems such as ZnO/CdS and SnO_2/CdS results in the quenching of the semiconductor emission.[35,40])

When adsorbed on a neutral surface such as silica, the major fraction of the decay can be fitted to single exponential with a lifetime of 124 ns. The initial fast decay component may arise from the excited state annihilation processes. However, when adsorbed on the SnO_2 surface, the excited state decays with a significantly faster rate. It should be noted that CdS-modified SnO_2 nanoclusters do not exhibit any detectable emission in the time scale chosen in our experiments. The charge transfer interaction between these two semiconductor systems results in the quenching of CdS emission.[40] The multiexponential

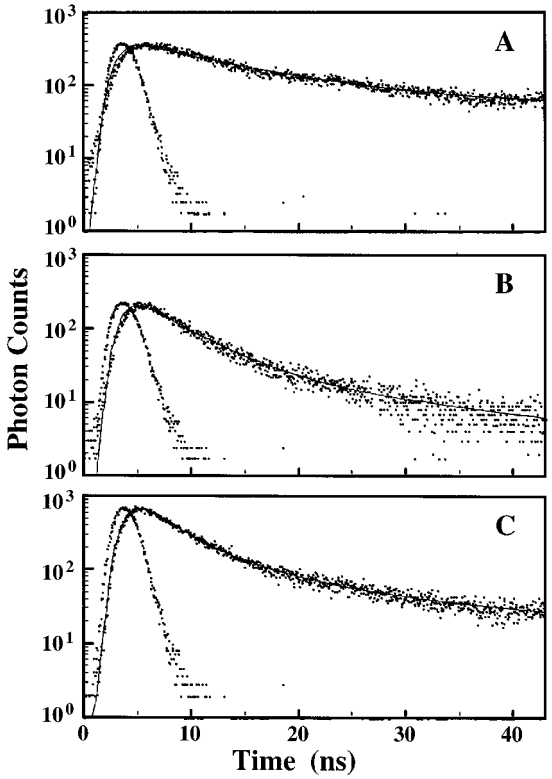

Figure 5. Emission lifetimes of (A) OTE/SiO_2/Ru(II), (B) OTE/SnO_2/Ru(II), and (C) OTE/SnO_2/CdS/Ru(II) (excitation 355 nm). Solid line shows the triexponential kinetic fit (eq 6). The laser profile is also shown for comparing instrument response time.

emission decay shown in Figure 5 were fitted using expression 6.

$$F(t) = a_1 \exp(-t/\tau_1) + a_2 \exp(-t/\tau_2) + a_3 \exp(-t/\tau_3) \quad (6)$$

The values of a_1, τ_1, a_2, τ_2, a_3, τ_3, and $\langle\tau\rangle$ are summarized in Table 1.

In our earlier study, we evaluated rate constants for the charge injection process from the luminescence decay of the sensitizer.[58] For SnO_2 film, the faster component had a rate constant of 3×10^8 s^{-1} and agreed well with the rate constant obtained from the pseudo-first-order growth of microwave conductivity. In order to employ a simplified analysis, we calculated an average lifetime based on the methodology of James et al.[59,60] The average lifetimes for SnO_2/Ru(II) and SnO_2/CdS/Ru(II) systems were 5.8 and 17.2 ns, respectively. If we assume the observed decrease in lifetime is entirely due to charge injection process, one could correlate the charge injection rate constant as

$$k_{et} = 1/\tau_s - 1/\tau_s^0 \quad (7)$$

where τ_s and τ_s^0 are the lifetimes of Ru(II)* on SnO_2 (or SnO_2/CdS) and silica, respectively. By substituting the values of τ_s^0 with 90 ns and τ_s with the average lifetimes of 5.8 and 17.2 ns, we obtain the values for k_{et} as 1.6×10^8 and 4.7×10^7 s^{-1} for SnO_2 and SnO_2/CdS films, respectively. The two values of k_{et} represent an apparent rate constant of net electron transfer from the excited Ru(II) into SnO_2 particles as observed in the present experiments.

The difference between the oxidation potential of excited sensitizer, Ru(II)* ($E^0 \approx -0.7$ V vs NHE) and the conduction band of the semiconductor provides a necessary driving force for the charge injection process (reaction 3). In the present case the driving force for the electron transfer to SnO_2 is positive and to CdS is slightly negative since their conduction bands are around 0.0 and -0.8 V vs NHE, respectively. We attribute the slower rate of electron transfer observed between Ru(II)* and CdS as compared to that between Ru(II)* and SnO_2 to the negative energy barrier. Despite this small energy barrier, the overlap between the excited state energy level of the sensitizer and the conduction band of the CdS is sufficient enough to induce the heterogeneous electron transfer at the semiconductor interface. The details on the dependence of electron transfer rate on the energy difference can be found in our previous studies.[50,58] Although the initial charge injection to CdS is slower, the subsequent propagation of injected electrons into SnO_2 particles is quick. The conduction band of SnO_2, which is around 0.0 V vs NHE, is expected to facilitate such a quick interparticle charge transfer. Transient absorption studies have confirmed that the electron transfer between the two semiconductor particles (e.g., CdS and TiO_2) is an ultrafast process and is completed within 2 ps.[39,61]

The multiexponential emission decay suggests that the charge injection in a nanocrystalline film is controlled by a distribution of charge transfer rate constants. The multiexponential decay behavior of excited Ru(II) complex observed in the present experiments arises from the different injection (active and inactive) sites and/or adsorption sites on SnO_2 surface. Evidence for the heterogeneity of the injection site has been presented by Xie and co-workers using far-field emission microscopy.[62]

Laser Flash Photolysis of Ru(II)-Modified Nanocrystalline SnO_2 and SnO_2/CdS Films. If indeed the emission quenching in Ru(II)-modified semiconductor films results in the charge injection process, we should be able to monitor the photoproduct (Ru(III)) of heterogeneous electron transfer process (reaction 3). The excitation of the Ru(II)-modified SnO_2 film was carried out in a front face geometry with a 532 nm laser pulse. Figure 6 shows the transient absorption spectra recorded 50 ns after the laser pulse excitation of OTE/SiO_2/Ru(II), OTE/SnO_2/Ru(II), and OTE/SnO_2/CdS/Ru(II) electrode samples. The energy of the laser excitation pulse was kept sufficiently low (5 mJ/pulse). High absorption of Ru(II) at 532 nm ($\sim$0.3) assured nearly 50% absorption of the incident laser pulse.

Excitation of the Ru(II) adsorbed on silica film resulted in the formation of a transient with absorbance maximum at 380 nm, a bleaching corresponding to the ground state depletion at 460 nm, and an isosbestic point at 397 nm. These spectral features matched the reported spectral characteristics of Ru(II)*.[55] The major component of this transient has a lifetime of 0.12 μs. Any contribution from the excited state annihilation or self-quenching process which is usually observed on surfaces such as silica was very small (<5%).

The transient spectrum recorded 50 ns after the 532 nm laser pulse excitation of OTE/SnO_2/Ru(II) and OTE/SnO_2/CdS/Ru(II) is significantly different. (It should be noted that 532 nm laser pulse excitation ensured selective excitation of Ru(II) since CdS and SnO_2 have negligible absorption at this excitation wavelength.) The lack of absorbance maximum at 380 nm indicates the decay of the excited state within the time period of 50 ns. However, a long-lived bleaching at 460 nm persists following the quenching of the excited state. This is indicative of the formation of the oxidation product, Ru(III). The bleaching observed at 397 nm (this wavelength corresponding to the isosbestic point of Ru(II)* and Ru(II) absorption) further confirms the fact that only the electron transfer product, Ru(III), contributes to the transient bleaching. Similar observation of Ru(III) formation in colloidal suspension has also been observed by us[63] and Ford and Rodgers[64−66] in colloidal SnO_2 suspensions.

TABLE 1: Emission Decay Kinetics of Ru(II) Complex Adsorbed on Different Nanocrystallites[a,b]

nanocrystallites	a_1	τ_1, ns	a_2	τ_2, ns	a_3	τ_3, ns	$\langle\tau\rangle$,[c] ns
SiO_2	0.006	10.2 ± 0.035	0.0011	11.2 ± 0.2	0.0014	123.9 ± 2.3	90
SnO_2	0.005	4.57 ± 0.06	0.0006	4.64 ± 0.45	0.0006	25.3 ± 0.58	5.8
SnO_2/CdS	0.016	3.33 ± 0.07	0.0042	10.73 ± 0.29	0.0006	124.5 ± 2.5	17.2

[a] The Ru(II) complex was adsorbed on different films that are cast on OTE. Measurements were made with dry films at room temperature using 355 nm laser pulse as the excitation source. [b] The emission decay was analyzed with a triexponential kinetic fit as described in eq 6. The CHISQR values were in the range 1.1−2.2. [c] See ref 60 for the determination of average lifetime, $\langle\tau\rangle$.

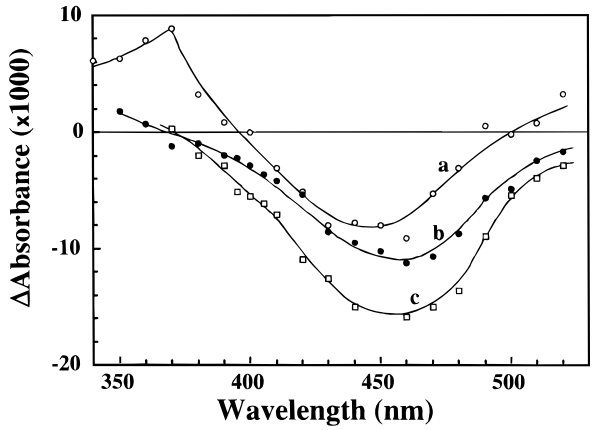

Figure 6. Transient spectra recorded 50 ns after laser pulse (532 nm) excitation of Ru(II) modified semiconductor thin films coated on OTE: (a) OTE/SiO_2/Ru(II) (○), (b) OTE/SnO_2/Ru(II) (●), and (c) OTE/SnO_2/CdS/Ru(II) (□).

Back Electron Transfer. In order to maximize the efficiency of net charge transfer, it is essential to suppress the loss of charge carriers due to back electron transfer between the injected charge and oxidized sensitizer (reaction 8).

$$\text{Ru(III)} + \text{SnO}_2\text{(e)} \xrightarrow{k_{ret}} \text{Ru(II)} + \text{SnO}_2 \qquad (8)$$

In a photoelectrochemical cell the back electron transfer is suppressed by regenerating the sensitizer with a suitable redox couple such as I_3^-/I^-.

$$2\text{Ru(III)} + 3\text{I}^- \rightarrow 2\text{Ru(II)} + \text{I}_3^- \qquad (9)$$

But it should be noted that the reaction 9 is in direct competition with the back electron transfer (reaction 8) and is usually overcome by employing high concentrations of redox couple. Although the back-electron-transfer rate constant is several orders of magnitude smaller than the rate constant for the charge injection process,[2,31,32,50] it does significantly increase with increase in the excitation intensity.[33,34] Hence, reaction 8 could be a major contributing factor in controlling the efficiency of net charge carrier accumulation within particles (or photocurrent generation).[33] If indeed the SnO_2/CdS semiconductor composite system has a beneficial effect in improving the charge separation efficiency, we should be able to see its influence directly on the back-electron-transfer process.

We extended the transient absorption study of Ru(II)-modified SnO_2 films to probe the back electron transfer between the injected charge and Ru(III) (reaction 8). The recovery of the bleaching recorded at monitoring wavelengths 400 and 460 nm for OTE/SnO_2/Ru(II) and OTE/SnO_2/CdS/Ru(II) is shown in Figure 7. These traces show that the reverse electron transfer is a multiexponential process. This multiexponential kinetic behavior arises from a distribution trap and/or surface sites that control the heterogeneous electron transfer at the semiconductor interface (reaction 8). Although it is difficult to analyze these

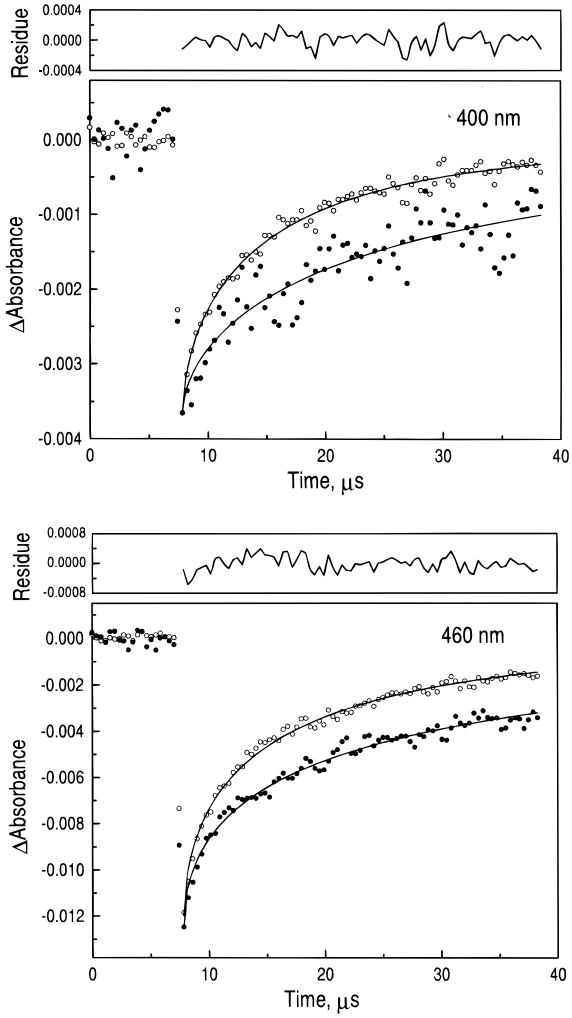

Figure 7. Absorption−time profiles at (A) 400 and (B) 460 nm recorded following the 532 nm laser pulse excitation of OTE/SnO_2/Ru(II) (○) and OTE/SnO_2/CdS/Ru(II) (●). The solid line shows the kinetic fit corresponding to the stretched exponential function (eq 10). The residue of the kinetic fit is also shown.

traces with simple decay kinetics, it is evident that the reverse electron transfer is completed over a period of 100 μs.

We analyzed these multiexponential decay using a stretched exponential kinetic function (Kohlrausch function).[67−70]

$$\Delta A(t) = \Delta A_0 \exp(-(t/\tau_K)^{\beta}) \qquad (10)$$

where β ($0 < \beta \leq 1$) is a stretching parameter that relates to a distribution of exponential decay times that are serially linked. As β increases, the distribution becomes narrower. Such an expression has been successfully applied by several researchers to analyze the multiexponential emission of semiconductors and the recovery of sensitizers on semiconductor and other heterogeneous surfaces.[58,66,71−74] This function models a system that relaxes with a distribution of exponential decay times whose peak value is close to the characteristic lifetime, τ_K. The solid

TABLE 2: Back Electron Transfer between Ru(III) and Electrons Injected in SnO_2 Nanocrystallites[a,b]

nanocrystalline film	monitoring wavelength	β	τ_k, μs	$\langle\tau_k\rangle$,[c] μs	$\langle k_{ret}\rangle$, 10^5 s^{-1}
SnO_2	400	0.62 ± 0.01	7.26 ± 0.13	10.52 ± 0.34	0.95 ± 0.03
	460	0.57 ± 0.01	8.17 ± 0.09	13.34 ± 0.04	0.75 ± 0.02
SnO_2/CdS	400	0.60 ± 0.04	19.56 ± 0.93	29.70 ± 3.35.	0.34 ± 0.04
	460	0.50 ± 0.01	16.41 ± 0.26	32.95 ± 1.17	0.30 ± 0.01

[a] The Ru(II) complex was adsorbed on SnO_2 and SnO_2/CdS films that were cast on OTE. The recovery of the bleached Ru(II) complex was monitored with dry films at room temperature using 532 nm laser pulse as the excitation source. [b] The transient absorption recovery was analyzed with a stretched exponential fit as described in eq 10. β is a stretching parameter, τ_k is a lifetime corresponding to the peak value and $\langle\tau_k\rangle$ is the average lifetime. The nonlinear curve fitting was carried out using the Marquadt−Levenberg expression from the Origin 4.1 software (Microcal Inc.). [c] Average lifetime $\langle\tau_k\rangle$ was determined from the expression[66,71−74] $\langle\tau_k\rangle = (\tau_k/\beta)\Gamma(\beta^{-1})$ where Γ is the gamma function.

lines in Figure 7 show the kinetic fit using expression 10. The lifetimes of recovery corresponding to the back electron transfer and the β values are summarized in Table 2. The β values are in the range 0.5−0.6, suggesting similar distribution of lifetimes in both these cases. Both the characteristic lifetime, τ_K, and average relaxation time, $\langle\tau_K\rangle$, which correspond to the back electron transfer in the Ru(II) modified films are summarized in Table 2.

The back-electron-transfer rate constants ($1/\langle\tau_K\rangle$) obtained from the transient recovery at 400 and 460 nm of SnO_2/CdS/Ru(II) films were 0.34×10^5 and 0.30×10^5 s^{-1}, respectively. The similarity between the two values suggests that the observed rate constants are wavelength independent and transient bleaching arise from the same species, viz., Ru(III). It may be noted that the bleaching at 460 nm could arise from both Ru(II)* and Ru(III) formation while the bleaching at 400 nm solely results from Ru(III) formation (400 nm is an isosbestic point for the absorption of ground and excited Ru(II)*). Thus, the comparison between the two traces allows us to exclude any contribution of Ru(II)* decay to the bleaching recovery traces in the time scale chosen for these studies.

The rate constant of back electron transfer obtained for SnO_2/CdS/Ru(II) film was smaller by a factor of 2−3 than the corresponding rate constant of SnO_2/Ru(II) film. This slower recovery of the transient bleaching seen at both monitoring wavelengths (400 and 460 nm) provides supportive evidence for the improved charge separation in the SnO_2/CdS composite films. The improvement in the charge rectification in SnO_2/CdS composite film thus accounts for the increased efficiency of charge carrier accumulation.

Arguments presented in an earlier study indicates that the rate constant for back electron transfer can also be minimized using an externally applied bias.[31,32] But for practical applications of photochemical solar cells, one needs to find alternate methods to suppress back electron transfer. In the present study the lower lying conduction band of SnO_2 nanocrystallites facilitates quick collection of photoinjected electrons and transfers them to the collecting surface of OTE to generate photocurrent. Ideally, one would hope to design a p−n-type composite semiconductor system for achieving maximum charge rectification. Nevertheless, the development of dye-modified composite semiconductor systems as described in the present study is another important step in this direction and provides new way to improve the performance of photochemical solar cells. Currently, efforts are underway to elucidate the role of sensitizer regeneration via I_3^-/I^- couple in single and multicomponent semiconductor films and how this regeneration step competes with the back-electron-transfer step.

Conclusions

Thin semiconductor films of composite semiconductor nanoclusters (SnO_2 and CdS) have been modified with a Ru(II) polypyridyl complex. The charge injection from excited sensitizer into CdS is followed by the transfer of electrons into SnO_2 particles. The charge rectification achieved in such composite semiconductor nanoclusters directly influences the photoelectrochemical properties of dye-modified semiconductor films. Higher photoconversion efficiency and slower back electron transfer observed with these composite semiconductor systems show their useful applications in photochemical solar cells and other light energy conversion devices.

Acknowledgment. We thank Richard Frankovic, Department of Electrical Engineering, for his assistance in recording SEM pictures. C.N. and S.H. acknowledge the support of Natural Sciences and Engineering Research Council of Canada. The work described herein was supported by the Office of Basic Energy Sciences of the U.S. Department of Energy. This is Contribution No. 3989 from the Notre Dame Radiation Laboratory.

References and Notes

(1) O'Regan, B.; Grätzel, M. *Nature (London)* **1991**, *353*, 737.
(2) Nazeeruddin, M. K.; Kay, A.; Rodicio, I.; Humphry, B. R.; Mueller, E.; Liska, P.; Vlachopoulos, N.; Grätzel, M. *J. Am. Chem. Soc.* **1993**, *115*, 6382.
(3) Meyer, G. J.; Searson, P. C. *Interface* **1993**, 23.
(4) Bedja, I.; Hotchandani, S.; Kamat, P. V. *J. Phys. Chem.* **1994**, *98*, 4133.
(5) Bedja, I.; Hotchandani, S.; Carpentier, R.; Fessenden, R. W.; Kamat, P. V. *J. Appl. Phys.* **1994**, *75*, 5444.
(6) Hotchandani, S.; Kamat, P. V. *Chem. Phys. Lett.* **1992**, *191*, 320.
(7) Hotchandani, S.; Das, S.; Thomas, K. G.; George, M. V.; Kamat, P. V. *Res. Chem. Intermed.* **1994**, *20*, 927.
(8) Liu, D.; Kamat, P. V. *J. Electrochem. Soc.* **1995**, *142*, 835.
(9) Nasr, C.; Hotchandani, S.; Kamat, P. V.; Das, S.; George Thomas, K.; George, M. V. *Langmuir* **1995**, *11*, 1777.
(10) Kamat, P. V. *CHEMTECH* **1995** (June), 22.
(11) Hagfeldt, A.; Grätzel, M. *Chem. Rev.* **1995**, *95*, 49.
(12) Memming, R. *Z. Phys. Chem. (Munich)* **1975**, *98*, 303.
(13) Clark, W. D. K.; Sutin, N. *J. Am. Chem. Soc.* **1977**, *99*, 4676.
(14) Hamnett, A.; Dare, E. M. P.; Wright, R. D.; Seddon, K. R.; Goodenough, J. B. *J. Phys. Chem.* **1979**, *83*, 3280.
(15) Ghosh, P. K.; Spiro, T. G. *J. Am. Chem. Soc.* **1980**, *102*, 5543.
(16) Dare, E. M. P.; Goodenough, J. B.; Hamnett, A.; Seddon, K. R.; Wright, R. D. *Faraday Discuss. Chem. Soc* **1980**, *98*.
(17) Breddels, P. A.; Blasse, G. *Ber. Bunsen-Ges. Phys. Chem.* **1982**, *86*, 676.
(18) Krishnan, M.; Zhang, X.; Bard, A. J. *J. Am. Chem. Soc.* **1984**, *106*, 7371.
(19) Dabestani, R.; Bard, A. J.; Campion, A.; Fox, M. A.; Mallouk, T. E.; Webber, S. E.; White, J. M. *J. Phys. Chem.* **1988**, *92*, 1872.
(20) Umapathy, S.; Hester, R. E. *Proc. Indian Acad. Sci., Chem. Sci.* **1990**, *102*, 613.
(21) Kim, Y. I.; Atherton, S. J.; Brigham, E. S.; Mallouk, T. E. *J. Phys. Chem.* **1993**, *97*, 11802.
(22) Bignozzi, C. A.; Argazzi, R.; Indelli, T.; Scandola, F. *Sol. Energy Mater.* **1994**, *32*, 229.
(23) Gerischer, H.; Willig, F. *Top. Curr. Chem.* **1976**, *61*, 31.
(24) Ryan, M. A.; Spitler, M. T. *J. Imag. Sci.* **1989**, *33*, 46.
(25) Hashimoto, K.; Hiramoto, M.; Kajiwara, T.; Sakata, T. *J. Phys. Chem.* **1988**, *92*, 4636.
(26) Hashimoto, K.; Hiramoto, M.; Lever, A. B. P.; Sakata, T. *J. Phys. Chem.* **1988**, *92*, 1016.
(27) Tani, T. *J. Imag. Sci.* **1990**, *34*, 143.
(28) Tani, T.; Suzumoto, T.; Ohzeki, K. *J. Phys. Chem.* **1990**, *94*, 1298.

(29) Ryan, M. A.; Fitzgerald, E. C.; Spitler, M. T. *J. Phys. Chem.* **1989**, *93*, 6150.
(30) Sonntag, L. P.; Spitler, M. T. *J. Phys. Chem.* **1985**, *89*, 1453.
(31) O'Regan, B.; Moser, J.; Anderson, M.; Grätzel, M. *J. Phys. Chem.* **1990**, *94*, 8720.
(32) Yan, S. G.; Hupp, J. T. *J. Phys. Chem.* **1996**, *100*, 6867.
(33) Liu, D.; Fessenden, R. W.; Hug, G. L.; Kamat, P. V. *J. Phys. Chem. B* **1997**, *101*, 2583.
(34) Ford, W. E.; Wessels, J. M.; Rodgers, M. A. J. Personal communication, 1997.
(35) Hotchandani, S.; Kamat, P. V. *J. Phys. Chem.* **1992**, *96*, 6834.
(36) Vinodgopal, K.; Kamat, P. V. *Environ. Sci. Technol.* **1995**, *29*, 841.
(37) Vinodgopal, K.; Bedja, I.; Kamat, P. V. *Chem. Mater.* **1996**, *8*, 2180.
(38) Spanhel, L.; Weller, H.; Henglein, A. *J. Am. Chem. Soc.* **1987**, *109*, 6632.
(39) Gopidas, K. R.; Bohorquez, M.; Kamat, P. V. *J. Phys. Chem.* **1990**, *94*, 6435.
(40) Kennedy, R.; Martini, I.; Hartland, G.; Kamat, P. V. *Sol. Energy Mater. Solar Cells*, in press.
(41) Rabani, J. *J. Phys. Chem.* **1989**, *93*, 7707.
(42) Kamat, P. V.; Patrick, B. Photochemistry and Photophysics of ZnO Colloids. Presented at the Symposium on Electronic and Ionic Properties of Silver Halides, Springfield, Va, 1991.
(43) Liu, D.; Kamat, P. V. *J. Electroanal. Chem. Interfacial Electrochem.* **1993**, *347*, 451.
(44) Liu, D.; Kamat, P. V. *J. Phys. Chem.* **1993**, *97*, 10769.
(45) Vogel, R.; Hoyer, P.; Weller, H. *J. Phys. Chem.* **1994**, *98*, 3183.
(46) Matsumoto, H.; Matsunaga, T.; Sakata, T.; Mori, H.; Yoneyama, H. *Langmuir* **1995**, *11*, 4283.
(47) Nasr, C.; Kamat, P. V.; Hotchandani, S. *J. Electroanal. Chem.* **1997**, *420*, 201.
(48) The new batch of SnO_2 colloidal suspension (15%) obtained from Alfa Chemicals consists of a different stabilizer than the one employed in this study from a previous batch.
(49) Saupe, G. B.; Mallouk, T. E.; Kim, W.; Schmehl, R. H. *J. Phys. Chem. B* **1997**, *101*, 2508.
(50) Kamat, P. V.; Bedja, I.; Hotchandani, S.; Patterson, L. K. *J. Phys. Chem.* **1996**, *100*, 4900.
(51) Federici, J.; Helman, W. P.; Hug, G. L.; Kane, C.; Patterson, L. K. *Comput. Chem.* **1985**, *9*, 171.
(52) Nagarajan, V.; Fessenden, R. W. *J. Phys. Chem.* **1985**, *89*, 2330.
(53) Vogel, R.; Pohl, K.; Weller, H. *Chem. Phys. Lett.* **1990**, *174*, 241.
(54) Nasr, C.; Liu, D.; Hotchandani, S.; Kamat, P. V. *J. Phys. Chem.* **1996**, *100*, 11054.
(55) Vinodgopal, K.; Hua, X.; Dahlgren, R. L.; Lappin, A. G.; Patterson, L. K.; Kamat, P. V. *J. Phys. Chem.* **1995**, *99*, 10883.
(56) Bedja, I.; Hotchandani, S.; Kamat, P. V. *J. Electroanal. Chem.* **1996**, *401*, 237.
(57) Argazzi, R.; Bignozzi, C. A.; Heimer, T. A.; Castellano, F. N.; Meyer, G. J. *Inorg. Chem.* **1994**, *33*, 5741.
(58) Fessenden, R. W.; Kamat, P. V. *J. Phys. Chem.* **1995**, *99*, 12902.
(59) James, D. R.; Liu, Y.-S.; de Mayo, P.; Ware, W. R. *Chem. Phys. Lett.* **1985**, *120*, 460.
(60) The average lifetime $\langle\tau\rangle$ was obtained from the expression $\langle\tau\rangle = (\sum(a_i\tau_i^2))/(\sum(a_i\tau_i))$.
(61) Zhang, J. Z.; O'Neil, R. H.; Roberti, T. W. *Appl. Phys. Lett.* **1994**, *64*, 1989.
(62) Lu, H. P.; Xie, X. S. *J. Phys. Chem. A* **1997**, *101*, 2753.
(63) Liu, D.; Hug, G. L.; Kamat, P. V. *J. Phys. Chem.* **1995**, *99*, 16768.
(64) Ford, W. E.; Rodgers, M. A. J. *J. Phys. Chem.* **1994**, *98*, 3822.
(65) Ford, W. E.; Rodgers, M. A. J. *J. Phys. Chem.* **1995**, *99*, 5139.
(66) Ford, W. E.; Rodgers, M. A. J. *J. Phys. Chem. A* **1997**, *101*, 930.
(67) Richert, R. *Chem. Phys. Lett.* **1985**, *118*, 534.
(68) Plonka, A. *Time Dependent Reactivity of Species in Condensed Media*; Springer-Verlag: New York, 1986.
(69) Siebrand, W.; Wildman, T. *Acc. Chem. Res.* **1986**, *19*, 238.
(70) Klafter, J.; Shlesinger, M. F. *Proc. Natl. Acad. Sci. U.S.A.* **1986**, *83*, 848.
(71) Linsey, C. P.; Patterson, G. D. *J. Chem. Phys.* **1980**, *73*, 3348.
(72) Leung, L. K.; Komplin, N. J.; Ellis, A. B.; Tabatabaie, N. *J. Phys. Chem.* **1991**, *95*, 5918.
(73) Meyer, T. J.; Meyer, G. J.; Pfennig, B. W.; Schoonover, J. R.; Timpson, C. J.; Wall, J. F.; Kobusch, C.; Chen, X.; Peek, B. M.; Wall, C. G.; Ou, W.; Erickson, B. W.; Bignozzi, C. A. *Inorg. Chem.* **1994**, *33*, 3952.
(74) Castellano, F. N.; Meyer, G. J. *J. Phys. Chem.* **1995**, *99*, 14742.